

Cosmology with gravitational lensing

S. M. Chitre^{†,**}, Y. Mellier^{*,#}, D. Narasimha[†] and B. Fort^{*}

[†]Department of Astronomy and Astrophysics, Tata Institute for Fundamental Research, Homi Bhabha Road, Mumbai 400 005, India

^{*}Institut d'Astrophysique de Paris, 98 bis Boulevard Arago, 75014 Paris, France

[#]Observatoire de Paris, DEMIRM, 61 avenue de l'Observatoire, 75014 Paris, France

Gravitational lensing effect is a classical prediction of general relativity, but its application to cosmology has been recognized only relatively recently. The technology-driven developments in observational cosmology have spurred gravitational lensing events to the forefront of astronomy and they serve as valuable tools for measuring the cosmological parameters, for probing the dark matter in the universe and for constraining the cosmic scenario of structure formation. We review the recent developments in this field, namely, the time-delay measurements, the masses of galaxies and clusters of galaxies and the cosmic shear.

THE gravitational deflection of light is one of the classical tests of Einstein's general theory of relativity which was verified by the measurement of bending of starlight grazing the sun's limb during the total solar eclipse expedition of 1919. The occurrence of a lensing event is due to the gravitational field of an intervening massive body like a star, a galaxy or a cluster of galaxies deflecting the light paths coming from a suitably aligned background source. This leads to a distortion of the position, size, shape and even intensity of the distant source. Typically, the observational signatures manifest as multiple images, with almost identical spectral characteristics and achromaticity, of a background compact source and arcs and almost complete ring-like image morphologies created by the reshaping of an extended source such as a galaxy by the lensing action of a foreground deflector. The diagnostic power of gravitational lenses is largely realized from the formation of multiple images, which have identical intrinsic properties.

The first multiply-imaged lens system, 0957 + 561, was reported by Walsh *et al.*¹. There has been substantial progress, largely because of the technological advances, over the past two decades and there have been various manifestations of strong lensing such as multiply-imaged (double, triple and quadruple) QSOs, complete or partial ring-like morphologies and giant arcs, linear features and arclets have been detected (cf. Blandford and Narayan²). The gravitational lensing phenomenon has now come to be widely recognized as a powerful diagnostic tool for studying a variety of

problems in astrophysical cosmology. The foregoing image morphologies become handy for inferring the sizes and masses of lensing galaxies and galaxy clusters and for revealing the amount and distribution of gravitating luminous and dark matter in the deflecting objects lying en route to a distant source³. The distinguishing feature of lens systems as a tool of physical cosmology is that the image morphology is largely controlled by the extent of mass distribution and not by its emission characteristics. The cluster lenses can also serve as giant cosmic telescopes by furnishing a magnified view of the distant universe and this should provide an access to dim sources which are below the sensitivity limits of the current flux-limited surveys. Furthermore, strong gravitational lensing events are expected to supply reasonable constraints on the values of the cosmological parameters like the Hubble constant, density parameter and the cosmological constant (cf. Kochanek⁴ and Narasimha⁵).

The gravitational lens is a special probe of the structures in the universe, because it responds to all the mass in compact objects, baryonic and non-baryonic, luminous and dark. This becomes specially important as a diagnostic of the formation and evolution of the galaxy-clusters and massive galactic halos. Further, the source we observe and the lens we probe would be located independent of each other. The distribution of matter in lensing objects will not, in general, be smooth and it should be possible to utilize the granularity arising from discrete objects like planets, stars and black holes in galaxies and their halos, as microlenses^{6,7}. This should be helpful in probing the compact continuum and emission line regions of lensed QSOs. The potential of microlensing effects has been demonstrated from the EROS/MACHO experiments which provide tight constraints on the exclusion diagram of the mass range of compact baryonic objects in the galaxy. It is, however, beyond the scope of this review to discuss at length these interesting projects. We will only focus on applications of gravitational lensing to large-scale structure and geometry of the universe.

Geometrical optics and mathematical formulation

A classical prediction of the general theory of relativity is that a light beam which passes at an impact parameter

^{**}For correspondence. (e-mail: chitre@astro.tifr.res.in)

distance b from a point mass M is deflected towards the body through an angle (in radians),

$$\varepsilon = \frac{4GM}{c^2 b}. \quad (1)$$

For a general mass distribution in a linearized theory, the bending angle is given by

$$\alpha = -\frac{2}{c} \int \nabla \Phi d\vec{r}, \quad (2)$$

where Φ is the Newtonian gravitational potential and the integral is along the photon path in the absence of any gravitational fields. It is generally the case that wavelengths involved are small enough compared to the Schwarzschild radius of the lensing object and the principle of geometrical optics may be adopted while treating the lensing action. Furthermore, the distances between the observer, deflector and source are large compared to the impact parameter, so that the bending angle has a negligible component along the light path. Consider a point source located at S whose light rays are deflected by a lens of mass M located at D before reaching the observer at O , as illustrated in Figure 1. Project the source and image positions onto a plane passing through the deflector and orthogonal to the sight-line to the source. Denoting the distances of the source and image positions from D by the vectors, \vec{r}_s and \vec{r}_i respectively, the lens equation relating the source and image positions may be written as⁸

$$\vec{r}_s = \vec{r}_i - \frac{\mu}{r_i^2} \vec{r}_i. \quad (3)$$

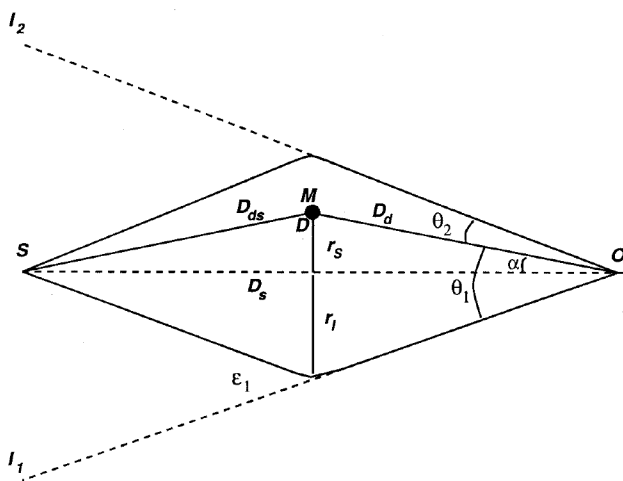


Figure 1. Schematic geometry of images of a point source S and a point mass deflector D as viewed by an observer O .

Here $\mu = \frac{4GM}{c^2} \frac{D_d D_{ds}}{D_s} \equiv \frac{4GM}{c^2} D_{\text{eff}}$ is a measure of the strength of lens of mass M . This can be expressed in angular coordinates as

$$\theta^2 - \alpha\theta - \theta_E^2 = 0. \quad (4)$$

Here

$$\theta_E = \left[\frac{4GM}{c^2} \frac{D_{ds}}{D_d D_s} \right]^{1/2}, \quad (5)$$

is the angular radius of the Einstein ring that sets the effective scale for the image separations and α is the angular displacement of the source S from the deflector D . For an arbitrary lens mass distribution, it would be useful to follow the scalar formalism developed by Schneider⁹ and Kovner¹⁰, which relates the source and image positions through the lens equation:

$$\vec{r}_s = \vec{r}_i - \nabla \phi(r_i), \quad (6)$$

where the effective gravitational potential ϕ , projected onto the deflector plane is determined through the two-dimensional Poisson equation,

$$\nabla^2 \phi = 2\kappa. \quad (7)$$

Here $\kappa = \Sigma / \Sigma_c$ is the convergence parameter representing the Ricci focusing and is proportional to $\Sigma(\vec{r}_i)$, the projected surface mass density. The critical surface mass density, $\Sigma_c = \frac{c^2}{4\pi G D_{\text{eff}}}$ governs the formation of multiple images and thus provides a geometrical method to estimate the cosmological parameters from the observation of strong lensing features like highly distorted images. The Weyl focusing is characterized by the non-local shear, γ and represents the distortion of the photon beam by the mass outside the photon path; it can be derived from the distribution of κ in the lens plane¹¹ and may be expressed as

$$\gamma = \begin{pmatrix} \gamma_1 \\ \gamma_2 \end{pmatrix} = \begin{pmatrix} \frac{1}{2}(\partial_{xx}\phi - \partial_{yy}\phi) \\ \partial_{xy}\phi \end{pmatrix}, \quad (8)$$

where ∂_{ij} denotes the partial derivative of the projected potential with respect to the coordinates ij . The amplification from the source to the image plane is then given by

$$A = \frac{1}{(1 - \kappa)^2 - \gamma^2}, \quad (9)$$

and the magnification matrix, which expresses the transformation between the image and the source plane, can be written as

$$A^{-1} = \frac{d\theta_s}{d\theta_I} = \begin{pmatrix} 1-\kappa-\gamma_1 & -\gamma_2 \\ -\gamma_2 & 1-\kappa+\gamma_1 \end{pmatrix}. \quad (10)$$

From this relation one can easily see that κ expresses an isotropic magnification of a lensed image, whereas γ provides the anisotropic shear which can produce a significant image distortion.

A complementary powerful theoretical formulation makes use of Fermat's principle, according to which light rays from a source to the observer travel along a path of extremal propagation time^{2,9,12,13}. The propagation time, in the presence of an intervening deflector, may be decomposed into two parts: (a) a geometrical time-delay caused by the extra path-lengths taken by the deflected light beams and (b) a potential time-delay due to the differences in gravitational potentials along paths from various images. The time-delay can be expressed as

$$\Delta t = t_{\text{geom}} + t_{\text{pot}} = \frac{1+z_L}{2c} \frac{D_d D_s}{D_{ds}} \|\bar{\theta}_I - \bar{\theta}_S\|^2 - \frac{2(1+z_L)}{c^3} \int \Phi(\theta_I) dl. \quad (11)$$

In this expression, z_L denotes the lens redshift, Φ the gravitational potential and $\bar{\theta}_S, \bar{\theta}_I$ are, respectively, the angular source and image positions. The extremal of the time-delay surface can then be studied for a given source position, to obtain the requisite information about image positions and time-delays between images.

The earlier theoretical studies were largely devoted to modelling of the multiply-imaged lens systems¹⁴. The thrust of such a direct method was to reproduce the observed image separations and intensity ratios for a given source-structure with an assumed lens model. Later, efficient inversion techniques like the Ring cycle, Lens Clean and Lens MEM methods were developed to reconstruct the source-structure from the observed image map^{15,16}. Of course, before undertaking a detailed theoretical modelling, it has been useful to make a qualitative classification of imaging geometry. This can be achieved with the help of the lens equation (eq. (3)) which represents a transformation from the image to the source plane and is generally a many-to-one mapping. The locus of the merging images is known as the critical curve, and the corresponding locus in the source plane is called the caustic which separates the regions of different image multiplicities. A source extending across the caustics forms a pair of merging images. The lens property close enough to a caustic is independent of the details of the lens models and can be gainfully analysed using the generic properties of the singularity. The caustic can be understood through a simple example of reflection of sunlight from the water in a pond.

For stagnant water, the surface of the water is plane and its bottom appears as it is. But if the surface is perturbed by a wave, we see a projection of this uneven surface in the reflected light and the shapes appearing in the reflection create the caustics of the mapping from the uneven water surface to the bottom of the pond. The gravitational lens acts in a similar way. From Fermat's principle, the time-delay surface due to the gravitational potential of the lens has an analogous role as the wavy surface of the water in the pond. Observation of the manifestation of these caustics, through the multiple images has provided a major breakthrough in cosmology in the last two decades. The source regions that cross a caustic are substantially magnified, a feature that has been profitably employed for carrying out the inversion procedure.

Time-delays and cosmological parameters

An unambiguous signature of a strong lensing event, apart from achromaticity, would be that if the intensity, polarization characteristic or any spectral feature of the original background source undergoes a change with time, these variations will not be reflected in all the images simultaneously. A relative time-delay between images is then expected, which will result from differences in geometrical path lengths and from varying gravitational potential wells traversed by the light beams from various images. The effective time-delay eq. (11) may be expressed as $\Delta t = \frac{1}{H_0} F(z_L, z_S, \text{lens model, cosmological model})$, with the dimensionless function F having a rather weak dependence on the underlying cosmological model, in particular, the density parameter and the cosmological constant. The time-delay is inversely proportional to the Hubble constant H_0 and has the largest uncertainty arising from the assumed lens model.

The multiply-imaged lens systems have been monitored over the years, both in the optical and radio wavebands, for recording the time-delays between components. Both the time-delay and redshift measurements are available for 5 lens systems which have been very extensively studied, yielding considerable amount of observational information (see Table 1).

These closely monitored gravitational lens systems appear to indicate that

- For an open universe with $\Omega_m = 0.2$ and $\Omega_\Lambda = 0$, $H_0 = 56 \pm 6 \text{ km s}^{-1} \text{ Mpc}^{-1}$.
- For a flat universe with $\Omega_m = 0.3$ and $\Omega_\Lambda = 0$, $H_0 = 66 \pm 6 \text{ km s}^{-1} \text{ Mpc}^{-1}$.

The lensing formalism evidently relies on a geometrical method that can measure cosmological distance-scales with no intermediate steps, unlike the conventional dis-

Table 1. Summary of robust time-delay measurements and the Hubble constant inferred from each monitoring

System	(z_S, z_L)	Time-delay (days)	Hubble constant (Ω_m, Ω_Λ)		Reference to observations
			(0.2, 0)	(0.3, 0.7)	
0957 + 561	(1.4, 0.36)	$\Delta t_{AB} = 423 \pm 3$	57 ± 10	66 ± 11	63
1115 + 080	(1.72, 0.31)	$\Delta t_{CB} = 25 \pm 4$ $\Delta t_{CA} = 14 \pm 5$ $\Delta t_{AB} = 11 \pm 5$	56 ± 12	64 ± 13	64
1830 – 211	(2.5, 0.89)	$\Delta t_{AB} = 28 \pm 6$	67 ± 16	80 ± 18	65
0218 + 357	(0.94, 0.68)	$\Delta t_{AB} = 11.7 \pm 0.9$	45 ± 9	53 ± 10	66
1608 + 656	(1.39, 0.63)	$\Delta t_{BA} = 31 \pm 7$ $\Delta t_{BC} = 36 \pm 7$ $\Delta t_{BD} = 76 \pm 10$	59 ± 12	63 ± 14	67

(z_S, z_L) refer to the redshifts of the source and the lens, respectively. The fourth column gives the Hubble constant for two popular cosmological models.

tance ladder. Admittedly, one needs to measure the time-delays for the multiply-imaged systems to better than 4% to constrain the value of H_0 within 10%. Nevertheless, with such an accuracy combined with direct measurement of the rotation velocity or the velocity dispersion of the lens galaxy, it should be possible to distinguish between, for example, a model with and without the cosmological constant. Systems like the triple quasar PG1115 + 080 would be good indicators of the Hubble constant, while B1608 + 656 or B0218 + 357 could provide constraints on the cosmological constant. There are observational as well as theoretical shortcomings, however, in all the foregoing systems. Thus, the twin quasar, 0957 + 561 has only two images and there may be two galaxy clusters in the field along the line of sight. The triple quasar, 1115 + 080 seems to exhibit a ratio of time-delays, Δt_{A-B} and Δt_{B-C} , which is inconsistent with a single lens component. By following the technique of data analysis developed by Narasimha⁵, this anomaly could be avoided, but the data appear to be degraded by the fluctuations in the calibrating star. The radio ring, 0218 + 357, for example, offers an attractive possibility for constraining the Hubble constant from the evidence for radio variability and highly variable polarization characteristics of the two compact flat-spectrum components. But the lens is probably a face-on spiral galaxy and there may not be a good way to estimate its bulge mass. In principle, it should be possible to overcome these difficulties with future observations of these and other well-constrained systems.

A challenging proposition is to look for transient sources like supernovae or gamma ray bursts in a high redshift galaxy that is being lensed by a foreground-rich cluster. The supernova event or the GRB and its afterglows should be revealed in distant multiply-imaged regions of the giant arc, which would be the manifestation of the background galaxy, but with a time-delay of

the order of several months to a year. With reasonable estimates of the cluster mass distribution and combining the information gleaned from the Sunyaev–Zeldovich effect, it should be feasible to derive a fairly reliable value of the Hubble constant.

The gravitational lensing statistics can also provide a valuable tool for determining the geometry of the universe, in particular to constrain the value of the cosmological constant. The available statistics on the distribution of lens redshifts and image separations have been effectively utilized to set an upper limit of $\Omega_\Lambda \sim 0.66$ at 95% confidence level^{4,17}. There are observations of multiple linear features as well as radial arcs in the field of rich galaxy clusters like Abell 1689, MS 2137, Abell 2390, Abell 2218 and C10024 + 17. For some of these (see Mellier¹⁸ for review), the multiband observational data as well as Sunyaev–Zeldovich results are also available. It is expected that accurate imaging as well as redshift measurements of the linear features in these systems can furnish a valuable insight into the nature of large-scale geometry of the universe. In particular, the information gained from the redshifts as well as separations between the breaks of three linear features can be profitably employed for estimating the luminous + dark matter density of the universe and even for determining the value of the cosmological constant for a specified cosmological model.

Probing the dark matter in the universe

All gravitating masses along the light paths, whether luminous or dark, baryonic or non-baryonic serve to act as lenses, provided the mass is concentrated in a sufficiently compact volume. The gravitational lensing effect is, therefore, ideally suited to detect mass-distributions in the universe, from planetary to super-cluster scales. The advantage of an independent location

of the tracer (lens) and the traced (source) helps to provide an unbiased probe of structures in the universe. It turns out that gravitational lensing phenomenon displays its most impressive and spectacular signature in its search for the dark matter.

The strong lensing phenomenon refers to configurations where lensed sources produce morphologies such as multiple images, arcs or rings. Although theoretically predicted earlier, the impact of the discovery of giant arcs in clusters of galaxies 15 years ago was considerable^{19–22}. They provided a new vision of clusters of galaxies with its tapestry of arcs of varying sizes:

- The typical angular scale of giant arcs detected in clusters suggests that dark matter dominates the cluster content and probably represents 90% of its total mass. This follows directly from the position of giant arcs, which must be close to the Einstein radius θ_E defined in eq. (5). For example, for a deflector at redshift 0.4, lensing a source at redshift 0.7, $\theta_E \approx 30''$ implying $M_{\text{cluster}}(r \leq \theta_E) = 1 - 2 \times 10^{14} M_\odot$, which is 10 times more than the mass contained in cluster galaxies.
- The existence of giant arcs in cores of rich clusters of galaxies suggests that the (dark) matter must be strongly concentrated towards the centre of lensing-clusters. This can be explained as follows: When the determinant of the magnification matrix (see eq. (10)) vanishes, the magnification becomes infinite. From an observational point of view, it corresponds to the formation of very extended images, like Einstein rings or giant arcs. They are formed only when the projected mass density is larger than a critical density,

$$\Sigma_{\text{crit}} \approx 0.1 \left(\frac{H_0}{50 \text{ km/sec/Mpc}} \right) \frac{d_{\text{os}}}{d_{\text{ls}} d_{\text{ol}}} \text{ g cm}^{-2}, \quad (12)$$

(written in appropriate scale for the angular distances). For example, for a lensing-cluster at redshift $z_L = 0.3$ and lensed sources at redshift $z_S = 1$, $d_{\text{os}}/(d_{\text{ls}} d_{\text{ol}}) \approx 3$. If the cluster can be modelled by an isothermal sphere with a core radius, R_c and with $M(R_c) = 2 \times 10^{14} M_\odot$, then, for $R_c = 250 \text{ kpc}$, $\Sigma(0) = 0.05 \text{ g cm}^{-2}$, and for $R_c = 50 \text{ kpc}$, $\Sigma(0) = 1 \text{ g cm}^{-2}$. The existence of giant arcs in clusters would then imply that dark matter in clusters should be strongly concentrated in the central region.

- A comparison between the dark matter distribution inferred from arcs and the light distribution of the brightest cluster galaxies shows that their geometrical properties (position, orientation, ellipticity) are similar. Therefore, inside clusters of galaxies, light does indeed, trace mass. (cf. Mellier¹⁸).

- Some lensing-clusters show multiple arcs with tangential as well as radial elongation with respect to the cluster centre (see Figure 2). For those exceptional cases, the use of these lens morphologies permits us to put tight quantitative constraint on the length-scale of the dark matter. In fact, these multiple lens systems have provided, for the first time, the typical sizes of core radii of dark matter distribution in clusters²³.
- Lastly, the simultaneous optical, X-ray and gravitational lensing observations provide us a handle to probe the amount and the distribution of both baryonic and non-baryonic matter in clusters as well as to compare their dynamical and thermodynamical state. This comparison led to the so-called X-ray/lensing mass discrepancy problem. It turns out that the masses of clusters of galaxies can also be inferred independently from the analysis of hot gas of protons and electrons which fills the intracluster medium.

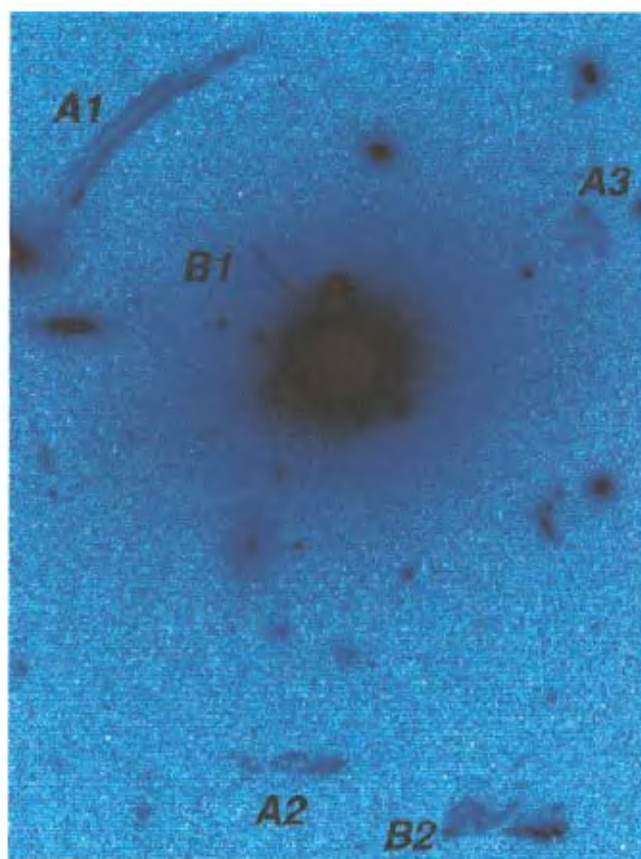


Figure 2. A spectacular strong lensing event in the cluster MS2137-23. Two arc systems are visible. The triple A-configuration shows a giant arc (A1) and its counter images (A2 and A3). The B-system is made by a radial arc (B1) and a counter image (B2) on the opposite direction. This system was modelled by Mellier *et al.*²³ who predicted the position and shape of A2–A3 and B2 prior to their detection.

The X-ray emissivity of this gas can be fitted to an empirical law which traces the shape of the mass density profile. By assuming this gas to be in hydrostatic equilibrium and the cluster to be a spherical system, one can infer a dynamical mass of the cluster which can be directly compared to its lensing mass. In many cases, the lensing-mass turns out to be about twice the X-ray-mass, although we expect them to be approximately the same. The projection effect along the line of sight can possibly overestimate the amount of cluster-material, although simulations indicate that this effect cannot be more than of 30% level. It is very likely that this discrepancy is an indication of the distribution and the dynamical stage of the hot gas being oversimplified. Remarkably, the X-ray clusters where cooling flows are present do not show a significant discrepancy between the X-ray and lensing mass, whereas other X-ray clusters do²⁴. This may be a consequence of the clusters with cooling flows being compact systems, which have perhaps virialized and have a well-defined relaxed core. In such a situation the assumption of hydrostatic equilibrium of the gas is satisfied. On the other hand, non-cooling flow clusters have lot of substructures and no dense core dominates the cluster. The physical state of gas in these systems may not obey a simple picture.

Far from the cluster centre, the gravitational lensing effect weakens progressively; but the gravitational field still acts to weakly distort the background galaxies. These weakly lensed galaxies produce a coherent pattern of correlated distribution of ellipticity/orientation which maps the projected surface mass density and which is clearly visible on deep CCD images (refs 25 and 26; Figure 3).

The weak lensing analysis assumes that the orientation of the sources is isotropic and that the redshift distribution of sources is known. It then proceeds along the following steps: (1) measurement of the averaged ellipticity and orientation of the galaxies inside all sub-areas of the field; (2) production of an ellipticity-orientation map (see Figure 3); (3) linking the ellipticity-orientation to the components of the shear; (4) correlating the shear with the mass density, and finally (5) relating the shape of sources to the shape of images.

The weak lensing analysis is based on the relations between shear, mass density and geometry of the lensed galaxies. When the shear is expressed as function of the gravitational convergence (see Seitz and Schneider²⁷ and references therein), the projected mass density can be recovered from measurement of ellipticities of the sources.

Although mass reconstruction is now a robust technique, the solution it provides is not necessarily unique, because the addition of a lens plane with constant mass

density keeps the distortion of galaxies unchanged. This is the so-called *mass sheet degeneracy*²⁸. The degeneracy could, in principle, be broken by measuring the magnification bias²⁹, which changes the galaxy number-

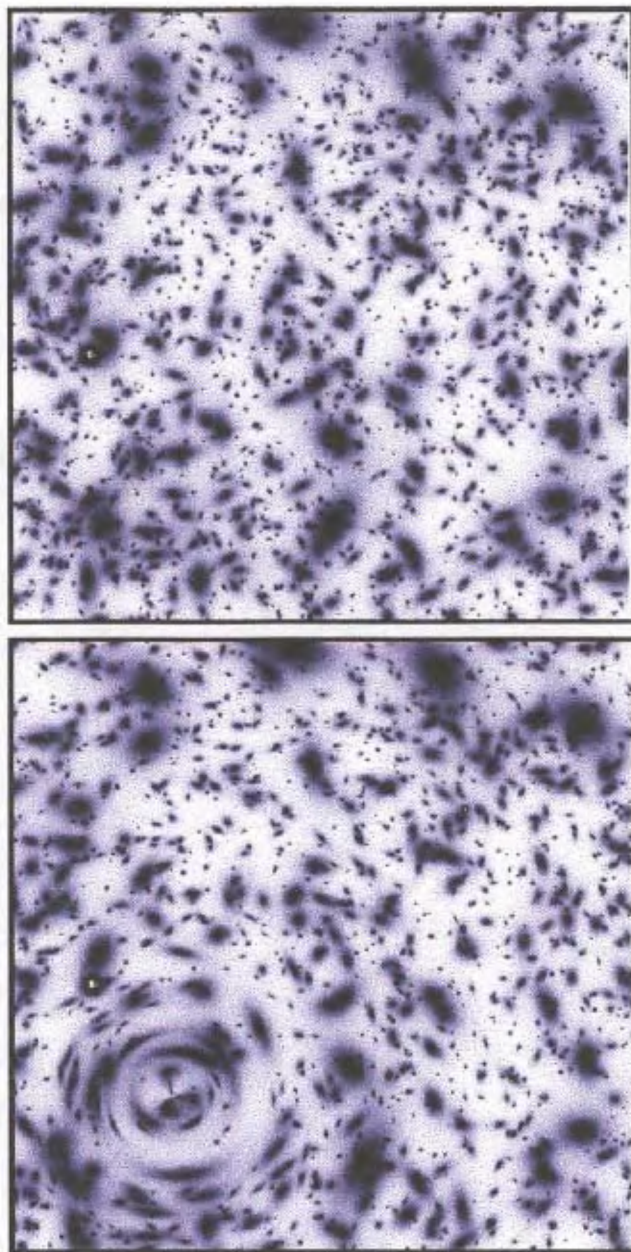


Figure 3. Distorted field generated by a lens. (Top panel) Grid of randomly distributed background sources as it would be seen in the absence of any lens. The projected number density corresponds to very deep exposure, similar to the HDF. (Bottom panel) Same population once they are distorted by a foreground (invisible) circular cluster with a typical velocity dispersion of 1300 km s^{-1} . The geometrical signature of the cluster is clearly visible. The potential can be recovered by using the formalism qualitatively explained in the text. In this simulation, the sources are at $z_s = 1.3$ and the cluster at $z_L = 0.15$.

counts. This bias is produced by the gravitational magnification, which increases the flux received from lensed galaxies and magnifies by the same amount the area of the projected lensed sky, which decreases the apparent galaxy number density. The total amplitude of the magnification bias depends on the slope of the galaxy number density as a function of magnitude and on the magnification factor of the lens. It can be shown that depending on the number density of lensed galaxies, one can observe an increase or a decrease in the number of galaxies behind the lensing-cluster. This property provides a measurement of the magnification and can be included in the mass reconstruction to break the mass sheet degeneracy.

Since 1990, many clusters have been investigated using weak lensing inversion techniques with ground-based or HST data. All these studies show that on scales of about 1 Mpc, the geometry of mass distributions, the X-ray distribution and the galaxy distribution is similar (see Figure 4), though the ratio of each component with respect to the others may vary with radius. The inferred median mass-to-light ratio, M/L , is about 300 (in solar units of M/L), with a trend to increase with radius. Contrary to the strong lensing cases, there is no evident discrepancy between the X-ray mass and the weak lensing mass.

From the investigation of about 20 clusters, it turns out that the median M/L is lower than 400. This implies that weak lensing analyses predict the density parameters $\Omega_m < 0.3$ with a high significance level. These constraints on Ω_m are in good agreement with other observations³⁰.

From strong and weak lensing analyses, we deduce the following features relating to mass distribution in galaxy-clusters:

- The presence of a substantial amount of dark matter as implied by a relatively large mass-to-light ratio M/L (greater than 200); (cf. Mellier¹⁸).
- The velocity dispersions inferred from optical observations and gravitational lensing are generally in reasonable accord. However, the scale-length of mass distribution inferred from strong lensing is typically of the order of 50 to 200 kpc, which is significantly smaller than the scale of galaxy distribution in the cluster^{22,31}.
- Several clusters exhibit subclustering on the scale of hundred kpc or so, which is manifest from the weak lensing analysis as well as from the discrepant velocity dispersion in a few systems. (cf. refs 31–33).

Significantly, gravitational lensing analysis reveals the presence of dark matter condensation at the centre of rich galaxy-clusters, even though the mass distribution in the outer regions follows that of the luminous galaxies.

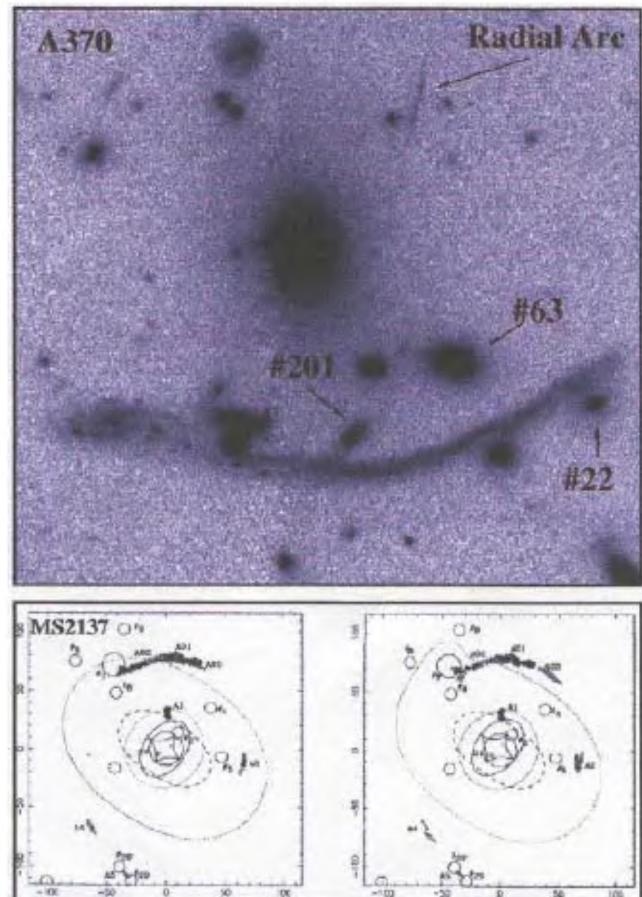


Figure 4. Perturbations close to giant arcs produced by galaxies. (Top panel) Giant arc in A370. The effects of the numbered galaxies, in particular that of the galaxy #22, on the giant arcs is clear in the HST images. (Bottom panel) Best lens model (left) of MS2137-23 and an example of the perturbation of the galaxy #7/(right). When too much mass is put in this galaxy one can see that the giant arc is broken in three sub-arcs. This effect permits us to put upper limits on the mass of this galaxy.

The mass reconstruction carried out by Luppino and Kaiser³⁴ and by Clowe *et al.*³⁵, and the detection of giant arcs in very distant clusters³⁶ indicate that massive clusters do exist at redshift ≈ 1 ! This is the first direct observational evidence that high mass-density peaks already have generated massive clusters of galaxies at redshift around $z = 1$; but the observational evidence about the total mass and the M/L ratio is still not very strong.

Measuring the masses of dark halos in galaxies

Gravitational lensing can provide valuable insights on the halos of galaxies. Since the lensing effect works on all scales, in principle, the halos of galactic dark matter could be probed from their gravitational lensing effects on background sources.

Dark halos in field galaxies

The gravitational lensing effect provides two reliable methods to estimate the scale length of dark halos around lensing galaxies, namely manifestation of Einstein rings and milliarcsecond scale jets (VLBI features) in multiple images. Rings occur when the observer, the lens and the source are almost perfectly aligned; if the source covers the whole of the internal caustic or extends over at least three cusps, the so-called 'Einstein ring' is formed. The first rings were observed around galaxies in radio surveys (see Refsdal and Surdej³⁷ for a review). The masses of the lensing galaxies can be very well constrained (see for instance Kochanek³⁸) from the position of the ring and fairly reliable properties of the halos may be inferred from models. The observed rings in various galaxy-lenses have diameters of the order of sub- to two arcseconds and the inferred scale length of mass distribution in field galaxies is larger than the scale of the luminous matter. But the velocity dispersion of the order of 150 to 300 km/s in almost all the cases and the mass-to-light ratio in the range of 8 to 30 are well within the values observed in local galaxies.

The mapping of VLBI features between the images proves to be a powerful method to infer mass distribution in the lens as well as to constrain the clumping of matter. The smooth transformation between the images of jets rules out the existence of appreciable number of black holes with masses of the order of a million solar masses. From the observations of many systems where the images of VLBI jets are nearly parallel, Narasimha and Chitre³⁹ inferred that the size of dark halos should be a few tens of kpc and their mass upwards of 10^{12} solar masses.

A promising approach to study the dark halos around field galaxies consists of a statistical study of the deformation of distant galaxies by foreground galactic halos. The galaxy-galaxy-lensing analysis uses the correlation between the position of foreground galaxies and the orientation of background population. We expect a deficit of radially-oriented galaxies and conversely an excess of tangentially-oriented images. If the correlation is produced by the gravitational shear of the foreground halos, then it is possible to probe their mass.

The expected gravitational distortion is very weak: for foreground lenses at redshift $\langle z_L \rangle = 0.1$, background sources at $\langle z_S \rangle = 0.5$ and typical halos with velocity dispersion of 200 km s^{-1} and radius of 100 kpc, $|\gamma| \approx 1\%$ at about 20 kpc from the centre. But if the observations go to very faint magnitudes, there is a huge number of background lensed galaxies, so that the weakness of the signal is compensated by the large statistics.

The first reliable results came from deep sub-arcsecond seeing CCD observations⁴⁰. Assuming a simple relation between the apparent luminosity of galaxies and their distances, the magnitude-mass relation pro-

vided by the Tully-Fisher empirical law was used to infer the typical mass and size of the dark halos. The prediction of the expected shear was compared with the observed polarization of about 1%, averaged over separation between $5''$ and $34''$ to rule out halos smaller than $10 \text{ h}^{-1} \text{ kpc}$ at a 2σ level, but the data are compatible with halos of sizes larger than $100 \text{ h}^{-1} \text{ kpc}$ and circular velocities of 200 km s^{-1} . Other surveys carried out after this pioneering work confirmed these results. In particular, the spectacular on-going massive redshift survey (the SLOAN project) of 2 million galaxies simultaneously has confirmed these results by reducing the error bars by a factor of 10 (ref. 41).

Dark halos in cluster member galaxies

Perturbations of caustics by intervening masses can locally change the length and shape of arcs or locally increase the intensity of unresolved arc substructures. Dramatic perturbations could even be responsible for the complete vanishing of an arc segment. If a large perturbation from a nearby galaxy is added, the image can be split into many components (Figures 2 and 4).

Large perturbations of caustics have been used to constrain the galaxies located close to the giant arcs in A370, Cl0024 + 17, Cl2244 or MS2137-23. In general, the absence of breaks along a well-defined arc provides robust upper limits to the masses of perturbing galaxies. The masses found for these cluster galaxies range between $10^{10} M_\odot$ and $2 \times 10^{11} M_\odot$, with typical mass-to-light ratios between 5 and 30.

Search for dark halos in the universe

One of the most effective uses of gravitational lenses is their role in searching astrophysical objects, with little or no emission contribution from their constituent baryons. It turns out that some dark halo candidates exist: These are cases of relatively large-separation image pairs like 2345 + 007, 1635 + 267 which have remarkably similar spectral characteristics^{42,43}. A few of such multiple-image configurations are likely to be a manifestation of dark gravitational lensing phenomena⁴⁴⁻⁴⁶. Equally, there are compelling theoretical reasons to invoke the assistance of an additional mass component around the lens galaxy, either in the form of a dark halo or as yet undetected compact core of a galaxy cluster for reproducing the observed large-separation image configurations³⁹. It is even tempting to speculate that massive under-luminous galaxies with dark halos are probably responsible for lensing action in some of the multiply-imaged systems with elusive intervening deflections. These may be huge ($M \geq 10^{12} - 10^{13} M_\odot$) low surface brightness (LSB) galaxies in the universe, situated at low-to-moderate redshifts, with inadequate star

formation. Such under-luminous objects may serve as dark lenses which could only be detected by the action of their gravitational fields on distant background sources.

A large quantity of neutral hydrogen present in such LSBs is liable to produce a copious amount of 21-cm radio emission with a flux of the order of a few tens of mJy. A substantial amount of 21-cm emission in the frequency range of 500 to 1400 MHz, for a range of lens redshifts, $z = 0.5$ – 1.5 , with the Ly α absorption at the same redshift will almost certainly clinch the hypothetical existence of dark massive lens galaxies and clusters!

More recently, a few candidates of ‘dark clusters of galaxies’ have been reported^{47–49}. Among these, the remarkable dark clump detected in the cluster A1942 from weak lensing analysis of two independent data sets using two different instruments and with observations separated by 3 years, is the most intriguing. The statistical analysis of the signal shows that the probability of such a high shear amplitude randomly occurring is less than 5×10^{-4} . Recent near infrared observations have also confirmed that there is no cluster at that position and unless deep X-ray observations are able to detect hot baryons, this would be a very convincing case for the presence of a dark cluster.

Large-scale structures and cosmic shear

The idea that mass condensations and the geometry of the universe can alter light bundles and distort the images of distant galaxies was emphasized by Gunn⁵⁰ and Blandford and Jaropszynski⁵¹. In the case of clusters, a change of the ellipticity distribution, namely a shear pattern, correlated with the mass distribution is expected as well. Since the expectation values strongly depend on the fraction of nonlinear systems and the redshift distribution of galaxies, it is clear that the analysis of weak lensing effects by large-scale structures is a challenging test of cosmological scenarios.

Theoretical expectations

The theoretical investigations of the effect of large-scale mass distribution on the ellipticity/orientation of distant galaxies are somewhat simplified by the low density contrast of structures. Beyond 10 Mpc scales, $\delta\rho/\rho \approx 1$ and the linear perturbation theory can be applied. On these scales, lenses are no longer considered individually; rather they are viewed as a random population which has a cumulative lensing effect on the distant sources. Blandford⁵², Blandford *et al.*⁵³, Miralda-Escudé⁵⁴ and Kaiser⁵⁵ first investigated the statistical distribution of distortions induced by large-scale struc-

tures in an Einstein–de Sitter universe. All these investigations concluded that the expected rms amplitude of the distortion is at the level of about one per cent.

More recently, Bernardeau *et al.*⁵⁶, used the perturbation theory in order to explore the sensitivity of the second and third moments of the gravitational convergence κ (rather than of the distortion whose third moment should be zero), to cosmological scenarios and particularly to cosmological parameters, including Λ -universes. They showed that in the linear regime, the cumulative effect of structures along the line-of-sight generates a convergence in the direction θ , whose variance $\langle \kappa(\theta)^2 \rangle$ and skewness $s_3 = \langle \kappa(\theta)^3 \rangle / \langle \kappa(\theta)^2 \rangle^{3/2}$ have the following dependencies with the cosmological quantities:

$$\langle \kappa(\theta)^2 \rangle^{1/2} \approx 10^{-2} \sigma_8 \Omega_0^{0.75} z_S^{0.8} \left(\frac{\theta}{1^\circ} \right)^{-(n+2)/2}, \quad (13)$$

and

$$s_3(\theta) \approx 40 \Omega_0^{-0.8} z_S^{-1.35}, \quad (14)$$

for a fixed source redshift z_S , where n is the spectral index of the power spectrum of density fluctuations and σ_8 the normalization of the power spectrum. Hence, since the skewness does not depend on σ_8 , the amplitude of fluctuations and Ω_0 can be recovered independently using $\langle \kappa(\theta)^2 \rangle$ and $s_3(\theta)$. Furthermore, the variance of the convergence at angular scale θ is also the variance of the shear. Since in the weak lensing regime the shear is obtained directly from galaxy ellipticity, these quantities are directly observable from the gravity-induced ellipticities of distant galaxies. It turns out that on small scales, where nonlinear structures dominate the weak lensing signal, the amplitude of the shear is about twice the theoretically expected value⁵⁷ making the observations easier than expected.

First detection of cosmic shear

The important scientific rewards expected from cosmic shear motivated many observational programmes in search of it. Although this is a technically and observationally very challenging task, four teams announced the detection of cosmic shear signal during the first semester of 2000: (1) van Waerbeke *et al.*⁵⁸ from a sample covering 1.6 deg^2 over 5 uncorrelated fields obtained at CFHT and Maoli *et al.*⁵⁹ on 45 VLT fields covering 0.5 deg^2 ; (2) Bacon *et al.*⁶⁰ from a sample of 14 fields obtained at WHT over 0.5 deg^2 ; (3) Wittman *et al.*⁶¹ from a sample covering 1.5 deg^2 over 3 uncorrelated fields at CTIO; and (4) Kaiser *et al.*⁶² from 6 fields at CFHT covering 1 deg^2 .

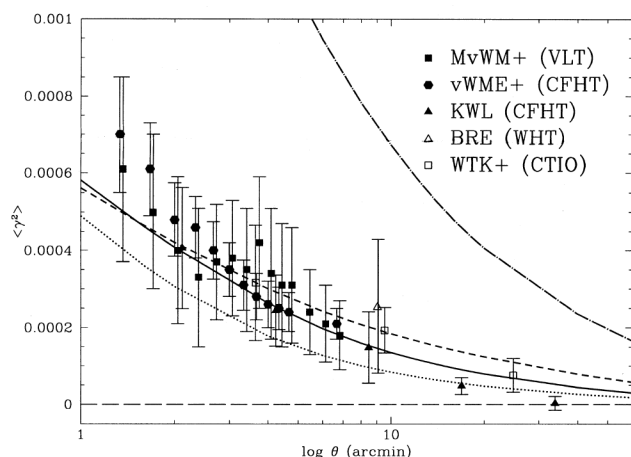


Figure 5. Recent results of cosmic shear measurements. Works referred to are Maoli *et al.*⁵⁹ (MvWM+), van Waerbeke *et al.*⁵⁸ (vWME+), Kaiser *et al.*⁶² (KWL), Bacon *et al.*⁶⁰ (BRE) and Wittman *et al.*⁶¹ (WTK+). Some predictions of cosmological models are also plotted, assuming sources at $z_{\text{eff}} = 1$. The solid line corresponds to Λ -CDM, with $\Omega_m = 0.3$, $\Omega_\Lambda = 0.7$, $\Gamma = 0.21$; the dot-dashed line to COBE-normalized SCDM; the dashed line to cluster-normalized SCDM and the dotted line to cluster-normalized open CDM with $\Omega_m = 0.3$.

The results are summarized in Figure 5. The most striking feature is that they are remarkably similar in the range $1'$ to $10'$. This is the crucial aspect which confirms that the detection and measurements are reliable and very robust, despite concerns about systematics. Furthermore, from this plot, one can already put constraints on cosmological scenarios. In particular, the SCDM COBE-normalized model is ruled out at least at a $5\text{-}\sigma$ level, and the popular Λ -CDM cluster-normalized model seems to fit data reasonably well.

The detection of the cosmic shear and the demonstrable reliability of the results obtained by various groups is being regarded as one of the most important results in cosmology last year. Indeed, it may put cosmic shear at the same level in observational cosmology as CMB and SNIa experiments. Among those, cosmic shear is the only one which probes directly the distribution of dark matter.

Future prospects

The spectacular developments in gravitational lensing underscore the need for new tools which can probe physical processes on gigaparsec scales and which are not biased by apparent structures of the universe inferred from the light of galaxies. The results described in this review serve to highlight its remarkable potential, but probably represent only a small fraction of what we can envision by way of its usage for the future. There are more surveys planned over the next decade. High resolution imaging and wide field surveys in

X-ray, optical, infrared and radio-wavelength are just beginning to provide terabyte data of the deep universe, which will contain thousands of new gravitational lenses. All those lenses will provide independent valuable constraints on the masses of galaxies, groups, clusters and superclusters of galaxies. Major scientific results are expected in three main topics: (1) dark matter distribution in gravitational systems; (2) cosmic shear, and (3) measurement of cosmological parameters.

Distribution of dark matter

The successful launch of the *Chandra* and XMM X-ray satellites is expected to soon provide superb images of giant galaxies and clusters of galaxies, which will enable us to resolve the X-ray/lensing mass discrepancy and to analyse in detail the distribution of baryons *vis-à-vis* non-baryonic matter, as well as their physical roles during cluster formation. But the most exciting goal is the search for dark halos. Should the dark halos of galaxies as well as dark clusters exist, then this will pose a fantastic challenge to theoretical cosmology and a remarkable confirmation of the uniqueness of gravitational lensing compared to any other technique using electromagnetic waves, to probe the universe (we are far from being able to use gravitational waves or neutrinos as detectors in cosmology).

Cosmic shear

Recent results on cosmic shear open a new window which will soon provide the variance and skewness of the convergence on the largest scale of mass distribution. Cosmic shear will then be able to provide independently the cosmological parameters and the normalization of the power spectrum and from the mass reconstruction of the projected mass density on degree-scale, the shape of the power spectrum of dark matter fluctuations. The cross-correlation between the luminous mass in galaxies and the dark matter will then provide invaluable information on the relation between the light and mass distribution (the 'biasing') and will permit an exploration of its evolution with angular scale and look-back time⁵⁸.

Cosmological parameters

The cosmic shear is not the only way to measure the couple of parameters, $(\Omega_m, \Omega_\Lambda)$. The light beams of multiply-imaged quasars cross the giant cosmological optical bench with angular separation which increases as Ω_Λ increases. The statistics of the fraction of quasars with large angular separation is therefore very useful to measure the cosmological constant. This approach suf-

fers from the poorly defined sample of quasars presently available. But the new spectroscopic surveys like SLOAN or 2dF will provide complete and well-defined sample of about 100,000 quasars.

Likewise, in lensing-clusters with multiple giant arcs with known redshifts, it is possible to infer the cosmological constant, provided the modelling of the lens is very well constrained. This approach is not reliable if one studies only one lensing-cluster. But the new, deep, wide-field optical and near infrared surveys will gather hundreds of candidates in order to infer Ω_Λ on a statistical basis.

Of equal importance, the measurement of the Hubble constant from time-delay measurements will also improve significantly. The incoming large sample of quasars will increase the number of candidates for monitoring by at least two orders of magnitude. Therefore, we should be able to infer H_0 with an accuracy better than 5%. It is important to keep in mind that compared to standard analysis, time delays provide H_0 on a cosmological scale, which is insensitive to local perturbation of the Hubble flow produced by gravitational interaction of our galaxy or the local group with other local systems. In this respect it should be, hopefully, more reliable.

Finally, we would like to mention that there is growing interest in the effect of gravitational lensing on the cosmic microwave background. Temperature fluctuation maps can be distorted by intervening structures in the same way as galaxies. These distortions are very interesting because the redshift of the source is perfectly known, namely $z = 1000$! At that redshift the universe is almost flat and the use of CMB data alone cannot distinguish between the values (Ω_m , Ω_Λ) corresponding to a flat universe. The simultaneous results of cosmic shear and CMB will break this intrinsic degeneracy. This is an original perspective where both CMB and gravitational lensing phenomenon work together to build up a single and coherent view of our universe.

All these developments are no longer dreams. The fantastic developments of ground- and space-based astronomy will make all-sky and multi-wavelength surveys possible immediately. We are now entering a new area of observational cosmology, where dark matter is no longer invisible.

1. Walsh, D., Carswell, R. F. and Weymann, R. J., *Nature*, 1979, **279**, 381.
2. Blandford, R. D. and Narayan, R., *Astrophys. J.*, 1986, **310**, 568–582.
3. Zwicky, F., *Phys. Rev. Lett.*, 1937, **51**, 290–292.
4. Kochanek, C. S., *Astrophys. J.*, 1996, **466**, 638–659.
5. Narasimha, D., *Cosmological Physics with Gravitational Lensing* (eds Mellier, Y. et al.), Les Arcs, 2000.
6. Paczynski, B., *Astrophys. J.*, 1986, **304**, 1–5.
7. Chitre, S. M. and Narasimha, D., in *Proc. of GR15* (eds Dadhich, N. and Narlikar, J. V.), 1997, pp. 1–22.
8. Saslaw, W. C., Narasimha, D. and Chitre, S. M., *Astrophys. J.*, 1985, **292**, 348–356.
9. Schneider, P., *Astron. Astrophys.*, 1985, **148**, 413–420.
10. Kovner, I., *Astrophys. J.*, 1987, **312**, 22–44.
11. Subramanian, K., Chitre, S. M. and Narasimha, D., *Astrophys. J.*, 1985, **289**, 37–51.
12. Kovner, I., *Astrophys. J.*, 1990, **351**, 114–120.
13. Nityananda, R., *Curr. Sci.*, 1990, **50**, 1044–1051.
14. Narasimha, D., Subramanian, K. and Chitre, S. M., *Mon. Not. R. Astron. Soc.*, 1982, **200**, 941–950.
15. Kochanek, C. S., Blandford, R. D., Lawrence, C. R. and Narayan, R., *Mon. Not. R. Astron. Soc.*, 1989, **238**, 43–56.
16. Wallington, S., Kochanek, C. S. and Koo, D. C., *Astrophys. J.*, 1995, **441**, 58–69.
17. Fukugita, M., Futamase, T., Kasai, M. and Turner, E. L., *Astrophys. J.*, 1992, **393**, 3–21.
18. Mellier, Y., *Annu. Rev. Astron. Astrophys.*, 1999, **37**, 127–189.
19. Soucaill, G., Fort, B., Mellier, Y. and Picat, J.-P., *Astron. Astrophys. Lett.*, 1987, **172**, L14–L17.
20. Lynds, R. and Petrosian, V., *Bull. Am. Astron. Soc.*, 1986, **18**, 1014.
21. Grossman, S. A. and Narayan, R., *Astrophys. J.*, 1988, **324**, L37–L40.
22. Narasimha, D. and Chitre, S. M., *Astrophys. J.*, 1988, **332**, 75–80.
23. Mellier, Y., Fort, B. and Kneib, J.-P., *Astrophys. J.*, 1993, **407**, 33–45.
24. Allen, S. W., *Mon. Not. R. Astron. Soc.*, 1998, **296**, 392–406.
25. Fort, B., Prieur, J.-L., Mathez, G., Mellier, Y. and Soucaill, G., *Astron. Astrophys. Lett.*, 1988, **200**, L17–L20.
26. Tyson, J. A., Valdes, F. and Wenk, R. A., *Astrophys. J. Lett.*, 1990, **349**, L1–L4.
27. Seitz, C. and Schneider, P., *Astron. Astrophys.*, 1996, **305**, 383–401.
28. Gorenstein, M. V., Falco, E. E. and Shapiro, I. I., *Astrophys. J.*, 1988, **327**, 693–711.
29. Broadhurst, T., Taylor, A. N. and Peacock, J., *Astrophys. J.*, 1995, **438**, 49–61.
30. Bahcall, N. A., *Phys. Scr.*, 2000, **85**, 32–36.
31. Kneib, J.-P. et al., *Astrophys. J.*, 1996, **471**, 643–656.
32. Tyson, J. A. and Fischer, P., *Astrophys. J. Lett.*, 1995, **446**, L55–L58.
33. Athreya, R., Mellier, Y., van Waerbeke, L., Fort, B., Pelló, R. and Dantel-Fort, M., *Astro-ph/9909518*, 1999 (accepted in *Astron. Astrophys.*).
34. Luppino, G. and Kaiser, N., *Astrophys. J.*, 1997, **475**, 20–28.
35. Clowe, D., Luppino, G. A., Kaiser, N., Henry, J. P. and Gioia, I. M., *Astrophys. J. Lett.*, 1998, **497**, L61–L64.
36. Deltorn, J.-M., Le Fèvre, O., Crampton, D. and Dickinson, M., *Astrophys. J. Lett.*, 1997, **483**, L21–L24.
37. Refsdal, S. and Surdej, J., *Rep. Prog. Phys.*, 1994, **56**, 117–185.
38. Kochanek, C. S., *Astrophys. J.*, 1995, **445**, 559–577.
39. Narasimha, D. and Chitre, S. M., *Astron. J.*, 1989, **97**, 327–335.
40. Brainerd, T. G., Blandford, R. D. and Smail, I., *Astrophys. J.*, 1996, **466**, 623–637.
41. Fischer, P. and the SDSS collaboration, *Astron. J.*, 2000, **120**, 1198–1208.
42. Weedman, D. W., Weymann, R. J., Green, R. F. and Heckman, T. M., *Astrophys. J.*, 1982, **255**, L5–L9.
43. Djorgovski, S. and Spinrad, H., *Astrophys. J.*, 1984, **282**, L1–L4.
44. Subramanian, K., Rees, M. J. and Chitre, S. M., *Mon. Not. R. Astron. Soc.*, 1987, **224**, 283–298.
45. Turner, E. L., Hillenbrand, L. A., Schneider, D. P., Hewitt, J. N. and Burke, B., *Astron. J.*, 1988, **96**, 1682–1689.
46. Steidel, C. C. and Sargent, W. L., *Astron. J.*, 1991, **102**, 1610–1626.

47. Bonnet, H., Mellier, Y. and Fort, B., *Astrophys. Lett.*, 1994, **427**, L83–L86.
48. Umetsu, K. and Futamase, T., Astro-ph/00043743, 2000.
49. Erben, T., van Waerbeke, L., Mellier, Y., Schneider, P., Cuilandre, J.-C., Castander, F. J. and Dantel-Fort, M., *Astron. Astrophys.*, 2000, **355**, 23–36.
50. Gunn, J. E., *Astrophys. J.*, 1967, **150**, 737–753.
51. Blandford, R. D. and Jaroszynski, M., *Astrophys. J.*, 1981, **246**, 1–12.
52. Blandford, R. D., *Q. J. R. Astron. Soc.*, 1990, **31**, 305–331.
53. Blandford, R. D., Saust, A. B., Brainerd, T. G. and Villumsen, J. V., *Mon. Not. R. Astron. Soc.*, 1991, **251**, 600–627.
54. Miralda-Escudé, J., *Astrophys. J.*, 1991, **380**, 1–8.
55. Kaiser, N., *Astrophys. J.*, 1992, **388**, 272–286.
56. Bernardeau, F., van Waerbeke, L. and Mellier, Y., *Astron. Astrophys.*, 1997, **322**, 1–18.
57. Jain, B. and Seljak, U., *Astrophys. J.*, 1997, **484**, 560–573.
58. van Waerbeke, L. *et al.*, *Astron. Astrophys.*, 2000, **358**, 30–44.
59. Maoli, R. *et al.*, Astro-ph/0008179, *Astron. Astrophys.*, 2001, **368**, 766–775.
60. Bacon, D., Réfrégier, A. and Ellis, R., Astro-ph/0003008, *Mon. Not. R. Astron. Soc.*, 2000, **318**, 625–640.
61. Wittman, D. M., Tyson, A. J., Kirkman, D., Dell’Antonio, I. and Bernstein, G., *Nature*, 2000, **405**, 143–148.
62. Kaiser, N., Wilson, G. and Luppino, G., *Astron. Astrophys.*, 2000, **303**, 27–40.
63. Kundic, T. *et al.*, *Astrophys. J.*, 1997, **482**, 75–82.
64. Schechter, P. L. *et al.*, *Astrophys. J.*, 1997, **475**, L85–L88.
65. Wiklind, T. and Combes, F., Astro-ph/9909314, 1999.
66. Biggs, A. D., Browne, W. A., Helbig, P., Koopmans, L. V. E., Wilkinson, P. N. and Perley, R. A., *Mon. Not. R. Astron. Soc.*, 1999, **304**, 349–358.
67. Fassnacht, C. D., Pearson, T. J., Readhead, A. C. S., Browne, I. W. A., Koopmans, L. V. E., Myers, S. T. and Wilkinson, P. N., *Astrophys. J.*, 1999, **527**, 498–507.

ACKNOWLEDGEMENTS. This work was supported by the CEFIPRA contract 1410-2. Y.M. thanks TIFR, Mumbai for hospitality where most of this review was completed. We thank L. van Waerbeke and F. Bernardeau for discussions.

Received 16 October 2000; revised accepted 2 January 2001

TECHNICAL NOTE

UNIVIS-2000: An indigenously developed comprehensive visualization package

Ajay C. Limaye^{*,†} and Shridhar R. Gadre^{†,**,†}

[†]Department of Chemistry, University of Pune, Pune 411 007, India

^{*}Australian National University Supercomputer Facility, Canberra, ACT 0200, Australia

This paper describes features of UNIVIS-2000, an indigenously developed MS-WINDOWS-based package for physicists, chemists and molecular biologists interested in modelling medium-sized molecules and visualization of molecular scalar functions defined over a regular grid or on a variety of molecular surfaces. The code is written in C⁺⁺ using freely available public domain graphics library, COSMO3D. The package provides essentially all the traditional features of molecular viewing softwares as well as visualization of scalar fields using planar pixel plots, contours and isosurfaces. A novel feature of UNIVIS-2000 is its ability to create composites of the functions, allowing scientists to quickly view an overall effect of one function over the other. For chemists, such a feature presents an opportunity to view the effect of one molecule on another with a change in their relative positions, providing valuable guidelines for exploration of molecular interactions without doing expensive calculations.

THE complexity of molecular systems engenders huge amounts of data generated by a variety of experiments or simulations. In view of this, visualization has become an invaluable tool for the modern chemist. There are several freely available packages^{1–8} for chemists that

allow viewing of molecules and a variety of molecular surfaces. Connolly⁹ has recently presented an excellent and comprehensive review of the computation and visualization of molecular surfaces.

UNIVIS-2000 is a visualization package for computational physicists, chemists and biologists who are not only interested in carrying out molecular modelling, but

^{**}For correspondence. (e-mail: gadre@chem.unipune.ernet.in)